crystals

MDPI

Article

Investigation of Preparation of Slag Wool from Melting-Separated Red Mud

Peipei Du [1], Yuzhu Zhang [1,2], Yue Long [2,*] and Lei Xing [2]

[1] School of Metallurgy, Northeastern University, Shenyang 110819, China; 1710508@stumail.neu.edu.cn (P.D.); zyz@ncst.edu.cn (Y.Z.)
[2] School of Metallurgy and Energy, North China University of Science and Technology, Tangshan 063009, China; xlncst@126.com
* Correspondence: longyue@ncst.edu.cn; Tel.: +86-15176503032

Abstract: The preparation of high-quality inorganic fibers by centrifugation from modified melting-separated red mud, which is the product of the efficient recovery of pig iron from red mud, is a new approach to achieve large-scale production of high value-added materials from red mud. This method has a wide range of application prospects and could contribute substantially to the comprehensive utilization of bulk industrial solid waste and the development of a circular economy. In this study, melting-separated red mud was modified with water-quenched blast furnace slag, quartz sand, and quicklime. The effect of the CaO/Na_2O mass ratio on the viscosity, fluidity, and crystallization performance of the melting-separated red mud was investigated; slag wool was prepared by centrifugation under laboratory conditions; and the effect of the CaO/Na_2O mass ratio on the morphology and properties of the slag wool was investigated. The viscosity of modified melting-separated red mud with different CaO/Na_2O mass ratios shows a decreasing trend with increasing temperature, and the fluidity increases with increasing temperature, indicating that the melt fluidity is improved. The suitable fiber-forming temperature of the melting-separated red mud shows a trend of increasing–decreasing–increasing with an increasing CaO/Na_2O mass ratio, and at a CaO/Na_2O ratio of 3.0, the maximum suitable fiber-forming temperature is 81 °C. Considering the feasibility of slag wool preparation from modified melting-separated red mud, the CaO/Na_2O of the modified raw material system should not be higher than 3.0. The crystallization temperature of modified melting-separated red mud with different CaO/Na_2O mass ratios first increases and then decreases, with a peak of 1450 °C at a CaO/Na_2O ratio of 4.0. Slag wool prepared from modified melting-separated red mud with different CaO/Na_2O mass ratios exhibits good properties, with a diameter of 5.47–6.67 μm and a slag ball content of 2.7–8.4%.

Keywords: melting-separated red mud; slag wool; CaO/Na_2O mass ratio; modification; centrifugal fiber formation

check for updates

Citation: Du, P.; Zhang, Y.; Long, Y.; Xing, L. Investigation of Preparation of Slag Wool from Melting-Separated Red Mud. *Crystals* **2023**, *13*, 1645. https://doi.org/10.3390/cryst13121645

Academic Editor: Pavel Lukáč

Received: 8 November 2023
Revised: 24 November 2023
Accepted: 27 November 2023
Published: 28 November 2023

Copyright: © 2023 by the authors. Licensee MDPI, Basel, Switzerland. This article is an open access article distributed under the terms and conditions of the Creative Commons Attribution (CC BY) license (https://creativecommons.org/licenses/by/4.0/).

1. Introduction

Red mud is a strongly alkaline industrial solid waste generated by alumina extraction in the aluminum industry; its output volume varies with ore grade, production process, and technology level, and at present, most manufacturers produce 0.8–1.5 t of red mud for every 1 t of alumina produced [1–3]. At present, the annual global output of red mud exceeds 100 million tons, and it is estimated that the current stockpile of red mud in China is approximately 800 million tons. As a typical bulk solid waste in the alumina industry, red mud has a comprehensive utilization rate of 20% or less [4,5]. The large amount of accumulated red mud not only occupies land resources but also can cause embankment failure in red mud reservoirs and soil and water pollution if not properly managed [6,7]. Melting-separated red mud is a slag byproduct of red mud after iron extraction; specifically, it is obtained after pig iron is extracted from Bayer red mud through

pretreatment with a coal-based reducing agent, reduction roasting, melting reduction, and separation. Melting-separated red mud is a byproduct of the extraction of valuable metal iron from red mud and is a form of solid waste remaining after primary resource use of red mud. Its main chemical components are Al_2O_3, SiO_2, Fe_2O_3, CaO, Na_2O, TiO_2, and MgO, with characteristic low iron, high aluminum, and high silicon contents, and it is a high-quality silicate material [8–10].

Slag wool is a cotton-like inorganic fiber material made by melting and fiberizing various types of industrial slag and other wastes [11,12]. It is lightweight, durable, non-combustible, noncorrosive, mold-resistant, and insect-resistant, and is an excellent thermal insulation and sound-absorbing material. Slag wool is mostly used for composite panels on the inner and outer walls of buildings, thermal and acoustic insulation for roofs, floor slabs and ground structures, and thermal insulation for industrial thermal equipment and refrigeration facilities [13–16]. The chemical composition of slag wool is generally as follows: SiO_2 (36–42%), Al_2O_3 (9–17%), CaO (28–47%), MgO (3–12%), Fe_2O_3 (1–5%), and small amounts of TiO_2, K_2O, and Na_2O [17]. The chemical composition of melting-separated red mud is similar to that of typical slag wool, and therefore, melting-separated red mud could be used as a raw material to prepare slag wool. Some studies have investigated the preparation of high-quality inorganic fibers from red mud. A methodology for carbothermically treating iron-bearing slags and by-products has been developed and tested on a semi-industrial scale by Balomenos et al. [18,19]. Thermodynamic modelling and conceptual design for processing bauxite residues (red mud) from the primary aluminium industry and ferro-nickel production slags are presented as examples. Furthermore, the results of semi-industrial-scale experiments for processing bauxite residues are illustrated, along with a preliminary financial analysis and an exergy flowsheet of the new conceptual alumina refinery, all confirming the financial viability as well as the resource-efficient utilization of the proposed technology. Kim Y et al. [20] used iron tailings, limestone, red mud, and nickel-iron slag to produce glass fibers at 1193–1230 °C, and the Young's modulus of the obtained fibers was 60–80 GPa. Chen ZW et al. [21] used thermodynamics calculations, a molecular dynamics simulation, and experiments to study the smelting reduction process, fiberization ability, and properties of mineral wool prepared from red mud; the results showed that the iron recovery rate exceeded 87%, the fiber formation rate from the slag was 73–92%, the average diameter of the obtained fiber was 1.57–5.62 μm, and the tensile strength of the fibers was 1520~6700 MPa. On the basis of a comparison of the composition of slag obtained from red mud after iron reduction and that of glass fibers, Bernd F et al. [22] designed a batch material for the production of glass fibers from iron-reduced slag and found that with the addition of 20–30% SiO_2, the prepared inorganic fibers were bright in color and had good mechanical strength, with a shape and appearance resembling those of mineral wool. The existing studies are mostly focused on theories and experiments on the preparation of inorganic fibers from red mud and additives, and there are relatively few studies on the preparation of inorganic fibers from melting-separated red mud. Our previous studies found that to prepare slag wool from melting-separated red mud, the composition of the slag wool should be reconstructed based on the principle of "silicon extraction, aluminum reduction, and calcium addition" [23]. Moreover, the bonding force between Ca^{2+} and non-bridging oxygen is different from that between Na^+ and non-bridging oxygen; the Na^+ bonding requires only one-half of the non-bridging oxygen, while Ca^{2+} bonding needs one non-bridging oxygen. Furthermore, Ca^{2+}, Si^{4+}, and Al^{3+} outcompete Na^+ for oxygen ions, while Na_2O provides oxygen ions with large polarization, which can moderate the competition of Ca^{2+}, Si^{4+} and Al^{3+} for oxygen ions and inhibit the destruction of the network structure of the slag wool. Therefore, in this study, the CaO/Na_2O mass ratio was chosen as a variable, and its effect on the viscosity, fluidity, and crystallization performance of melting-separated red mud was investigated. The aims were to establish qualitative and quantitative design parameter standards for the reconstruction of melting-separated red mud components, to improve the theory of melting-separated red mud modification for the preparation of high-quality inorganic

fibers, and to provide a theoretical basis for the precise modification of melting-separated red mud to prepare high-quality slag wool.

2. Materials and Methods

2.1. Experimental Materials

The melting-separated red mud used in the experiments was obtained from the Aluminum Corporation of China Limited. The particle size was in the range of 3–5 mm, and the sample was ground to 200 mesh for later use. The melting-separated red mud was combined with water-quenched blast furnace slag at a ratio of 2:1, after which quicklime (CaO) was introduced to adjust the CaO/Na_2O mass ratio of the system. The water-quenched blast furnace slag and quicklime were all taken from a steel mill in Tangshan City, Hebei Province. The chemical components of the melting-separated red mud, water-quenched blast furnace slag, and quicklime were determined by X-ray fluorescence (XRF) and are shown in Table 1.

Table 1. Chemical composition of melting-separated red mud, water-quenched blast furnace slag, quartz sand, and quicklime (mass ratio, %).

Raw Material	Al_2O_3	SiO_2	CaO	Na_2O	TiO_2	Fe_2O_3	MgO	K_2O	MnO	Other
Melting-separated red mud	32.31	27.26	10.62	11.16	7.23	7.56	2.14	0.30	0.13	1.29
Water-quenched blast furnace slag	14.47	28.32	38.72	0.32	2.16	--	11.28	0.46	0.38	3.89
Quicklime	--	1.28	90.0	--	--	--	1.56	--	--	7.16

The CaO/Na_2O mass ratios of the modified melting-separated red mud obtained after adding the water-quenched blast furnace slag are 2.6, 3.0, 4.0, and 5.0, with increments of 0.4 and 1.0 between the selected ratios. Table 2 shows the chemical compositions of the melting-separated red mud samples with different CaO/Na_2O mass ratios.

Table 2. Chemical composition of melting-separated red mud samples with different CaO/Na_2O mass ratios (mass ratio, %).

CaO/Na_2O	Quicklime	Chemical Composition									
		SiO_2	Al_2O_3	CaO	Na_2O	TiO_2	Fe_2O_3	MgO	K_2O	MnO	Other
2.6	0	27.61	26.36	19.98	7.55	5.54	5.04	5.19	0.35	0.21	2.17
3.0	2.88%	26.86	25.60	22.00	7.33	5.38	4.89	5.08	0.34	0.21	2.31
4.0	10.20%	24.92	23.67	27.12	6.78	4.98	4.52	4.82	0.32	0.19	2.68
5.0	16.49%	23.27	22.01	31.53	6.31	4.63	4.21	4.59	0.70	0.29	2.46

2.2. Analysis of Macroscopic Properties of Modified Melting-Separated Red Mud

The viscosity was measured using a comprehensive physical property analyzer (RTW-13, Northeastern University). The instrument constants were calibrated at room temperature using silicone oil, and a graphite crucible with molybdenum plates on the inner wall was used. A sample (140 g) was weighed and loaded into the graphite crucible. The crucible with the sample was placed in the analyzer and heated. After the temperature reached 1500 °C, the mixture was kept at 1500 °C for 30 min. Then the viscosity was measured at varying temperatures, with a temperature drop step size of 3 °C·min^{-1}.

According to the obtained chemical composition of the melting-separated red mud, the SiO_2-Al_2O_3-CaO-Na_2O-TiO_2 five-element slag system was taken as the research subject, and the Equilb module and Phase Diagram module in FactSage8.0 thermodynamics software, the FToxid database, and the Scheil–Gulliver cooling model were used to study the conversion pattern, the temperature of the onset of crystallization, and the dominant phase at the temperature of the onset of crystallization during the high-temperature cooling of modified melting-separated red mud [24]. During the simulation process, the melt temperature starts to cool from 1500 °C, with a cooling rate of 1 °C/min.

X-ray diffraction (XRD) analysis was performed on the water-quenched modified melting-separated red mud. A small sample with a particle size of less than 200 mesh was placed in a glass groove for sample preparation. The prepared samples were then placed into an X-ray diffractometer (D/MAX2500PC03030502, Rigaku Co., Ltd., Tokyo, Japan) to analyze their mineral phase composition. The working conditions of the X-ray diffractometer were as follows: CuKα radiation, tube voltage 40 kV, tube current 100 mA, scan speed 10° min^{-1}, and scan angle range 10–90°. Qualitative analysis of the XRD patterns was performed using Jade 6.5 software.

Field emission scanning electron microscopy (FESEM) was adopted to observe the micromorphology of the water-quenched modified melting-separated red mud. Before FESEM analysis, the sample was first prepared with conductive adhesive on a sample holder and then sprayed with gold using a JEC-3000FC fully automated sputter coater (JEOL Ltd., Tokyo, Japan.).

2.3. Preparation and Performance Characterization of Slag Wool

The slag wool was prepared by centrifugation under laboratory conditions. The equipment included a 100 kg DC electric arc furnace, a four-roller centrifuge, and wool collection equipment. The electric arc furnace lining was made of aluminum magnesium spinel refractory material, with a rated power of 100 kW. Figure 1 shows a schematic diagram of the experimental equipment and the fiberization process. Each batch experiment consisted of a furnace pre-heating stage (add 1.5 kg of coke to the electric furnace, lay the furnace bottom evenly, lower the electrodes, and start heating, approximately 1 h long), followed by feeding of the raw material through a feeder tube at the side of the furnace, at a rate of approximately 5 kg/min. The temperature on the internal of the melt produced was measured with a pyrometer couple. Then the temperature on the internal of the melt was set to 1500 °C, and it was held for 30 min until it was completely homogenized. Then the molten slag slowly flowed out from the electric arc furnace to the four-roller centrifuge for fiber formation [18]. The rotation speeds of rollers #1, #2, #3, and #4 were 4060 r/min, 4640 r/min, 5220 r/min, and 5800 r/min, respectively. The inorganic fibers were collected in a wool collection room. After the melt drops to the surface of the roller, due to the viscous force, a melt boundary layer with a large internal velocity gradient is formed, the melt flows around the roller to form a liquid film layer, and at the same time, bulges are formed in the liquid film, which are broken into fibers by the centrifugal force generated by the rotation of the roller.

Over 1 g of inorganic fibers was collected to prepare several samples of suitable size. A sample of approximately 1 mm was prepared by cutting and placed on a slide, an appropriate amount of immersion solution was added, and a needle was used to homogenize the fibers. A total of 100 fibers on the glass slide were measured by the microscope, and the calculated average diameter of the 100 fibers was used as the diameter of the inorganic fiber. In the slag ball content tester, the buoyancy effect of water is used to separate the inorganic fiber from the slag ball; thereby, the slag ball content in the inorganic fiber can be calculated as shown in Equation (1).

$$\omega = \frac{m}{m_0} \times 100 \quad (1)$$

where ω is the slag ball content in the inorganic fiber, %; m is the mass of the slag ball, g; and m_0 is the total mass of the sample, g.

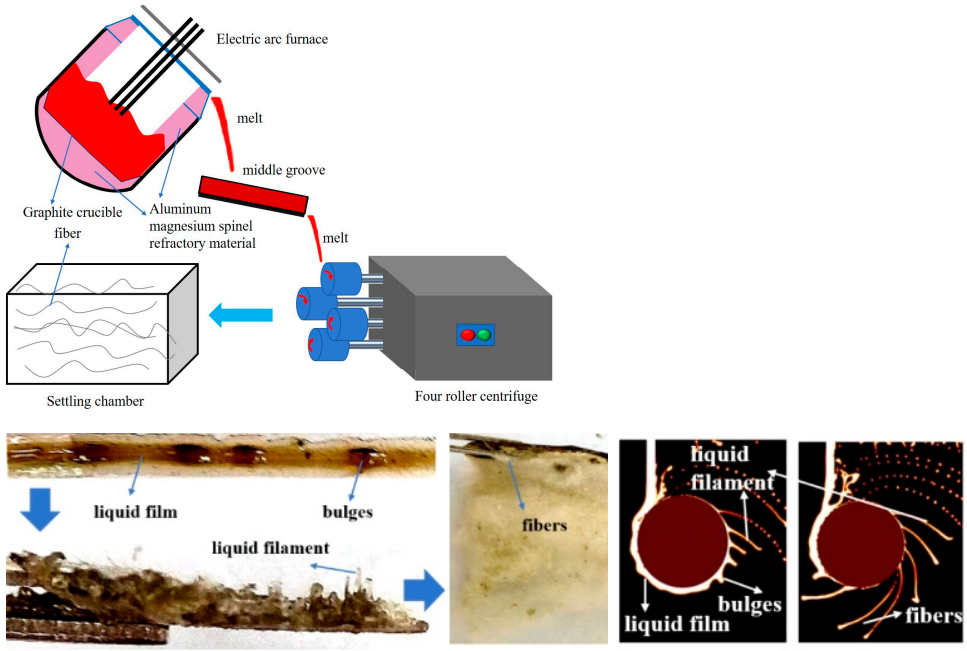

Figure 1. Schematic diagram of the experimental setup and the fiberization process.

3. Results and Analysis

3.1. Viscosity and Fluidity

The fiberization of modified melting-separated red mud involves the quenching of a high-temperature melt, which requires the melt to have good fluidity and low viscosity. Figure 2a shows the viscosity–temperature curves of modified melting-separated red mud with different CaO/Na_2O mass ratios. Figure 2a shows that the viscosity of the modified melting-separated red mud samples with different CaO/Na_2O mass ratios increases with decreasing temperature. With increasing CaO/Na_2O, the melt viscosity–temperature curve shows a smooth and slow change trend; this is consistent with the study by E.T. Turdogan et al. [25] on glass transition temperatures. In the high-temperature region (temperature > 1446 °C), at the same temperature, the melt viscosity gradually decreases with increasing CaO/Na_2O.

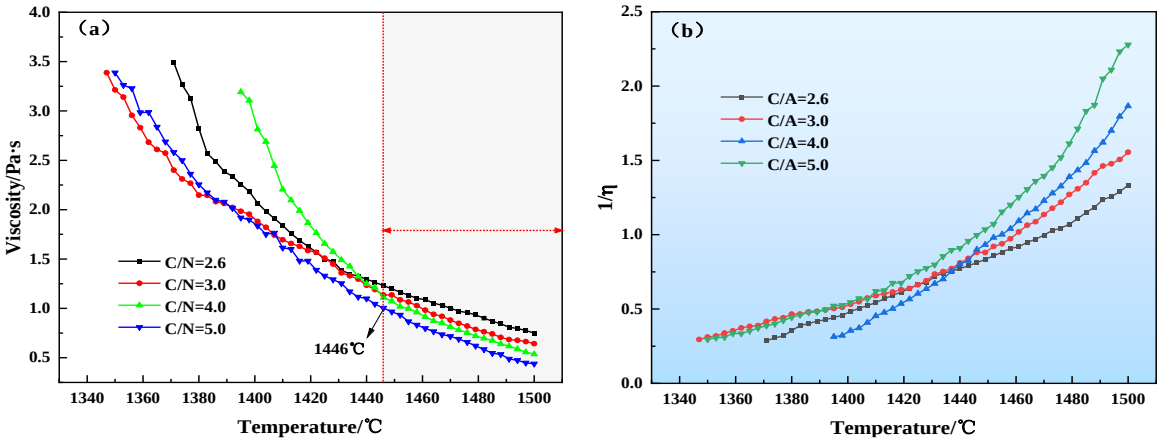

Figure 2. Viscosity–temperature curves and $1/\eta$-temperature curves of modified melting-separated red mud with different CaO/Na_2O ratios. (**a**) Viscosity–temperature curves; (**b**) $1/\eta$-temperature curves.

According to the continuous random network (CRN) model [26], in modified melting-separated red mud, the effect of Na^+ on the polarization of bridging oxygen and weakening

of the Si(Al)-O bond is stronger than that of Ca^{2+}, and the Na_2O in the melt provides more polarized oxygen ions to alleviate the competition of Ca^{2+} with Si^{4+} and Al^{3+} for oxygen ions. With an increasing CaO/Na_2O ratio, the CaO content in the melt increases, the Na_2O content decreases accordingly, the concentration of oxygen ions with high polarizability decreases, the complex silicate network structure in the melt are destroyed [27], the competition of Ca^{2+} with Si^{4+} and Al^{3+} for oxygen ions intensifies, and the network structure breaks down to form the "small molecule" polymer Si(Al)-O-Ca(Na). Moreover, the Ca^{2+} has a certain cumulative effect on the structure, causing violent motion of the "small molecule" polymer, and the viscosity of the modified melting-separated red mud decreases continuously.

The reciprocal of the viscosity $\varphi = 1/\eta$ is used to characterize the ease of melt flow and is called the melt fluidity. The higher the fluidity is, the better the melt fluidity. The variation curves of the fluidity ($\varphi = 1/\eta$) of modified melting-separated red mud samples with different CaO/Na_2O ratios with temperature are shown in Figure 2b. Figure 2b shows that the fluidity of modified melting-separated red mud with different CaO/Na_2O ratios increases as the temperature increases, indicating that the fluidity is improved; in the high-temperature region (temperature > 1446 °C), at the same temperature, the melt fluidity increases with an increasing CaO/Na_2O ratio, indicating that the fluidity is improved. With an increasing CaO/Na_2O ratio, the increase in Ca^{2+} in the modified system makes the viscous flow unit of the melt change from the Si(Al)-O-Si(Al) ionic group to the Si(Al)-O-Ca ionic group, and the melt network structure breaks into shorter chains of smaller size; at high temperatures, the motion of the Ca^{2+} and Si(Al)-O-Ca ionic groups in the voids of the melt structure is intense, and the melt fluidity increases, indicating that the fluidity is improved.

According to our previous research results [28], considering the energy consumption of the process, the raw materials used for slag wool preparation generally have a melt viscosity of 1 Pa·s or higher and have good fluidity; that is, the melt temperature should be above the melting temperature (the temperature at which the melt can freely flow, T_m). The melting temperature of melting-separated red mud can be obtained from the tangent point of the viscosity–temperature curve and the 45° tangent line. Figure 3a shows the melting temperature and the temperature at a viscosity of 1 Pa·s of modified melting-separated red mud with different CaO/Na_2O ratios, and the suitable fiber-forming temperature intervals are shown in Figure 3b. The temperature corresponding to a viscosity of 1 Pa·s is higher than the melting temperature, and in the temperature range corresponding to a viscosity greater than 1 Pa·s, the suitable fiber-forming temperature interval for modified melting-separated red mud shows a trend of increasing–decreasing–increasing with an increasing CaO/Na_2O ratio. The maximum suitable fiber-forming temperature interval was obtained at a CaO/Na_2O ratio of 3.0, with a value of 81 °C. When the CaO/Na_2O increases from 3.0 to 4.0, the suitable fiber-forming temperature interval suddenly decreases to 10 °C, and when the CaO/Na_2O is 5.0, the suitable fiber forming formation increases to 61 °C. Considering the feasibility of preparing slag wool from modified melting-separated red mud, the CaO/Na_2O ratio of the modified raw material system should not be higher than 3.0.

Within the suitable temperature range for fiber formation from modified melting-separated red mud, the movement of each particle in the melt is controlled by its surrounding particles, and only when a particle has enough energy (ΔE) to overcome the attraction by surrounding particles can it effectively migrate, exhibiting macroscopic fluidity. The more activated particles there are, the higher the fluidity. The relationship between the viscosity and temperature of modified melting-separated red mud can be characterized by the Arrhenius Equation (2) [29].

$$\eta = \eta_0 e^{\frac{\Delta E}{kT}} \quad (2)$$

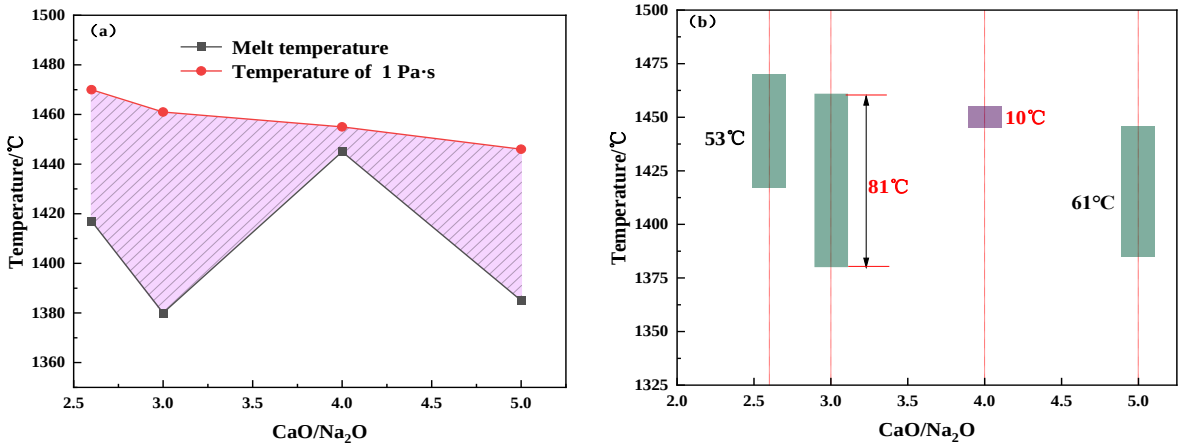

Figure 3. Temperatures at feature points and suitable fiber-formation temperature intervals of modified melting-separated red mud samples with different CaO/Na_2O ratios. (**a**) Temperatures at feature points; (**b**) Suitable fiber-formation temperature intervals.

In Equation (2), ΔE is the viscous-flow activation energy of the particles in the melt, $J{\cdot}mol^{-1}$; η_0 is a constant related to the melt composition; k is Boltzmann's constant, $J{\cdot}K^{-1}$; and T is absolute temperature, K.

Taking logarithms on both sides of Equation (2):

$$\ln \eta = \ln \eta_0 + \frac{\Delta E}{k}\frac{1}{T} \tag{3}$$

From Equation (3), $\ln\eta$ and $1/T$ are linearly related, and the slope of the line is $\Delta E/k$.

According to the suitable fiber-forming temperature intervals of modified melting-separated red mud samples with different CaO/Na_2O ratios, the relationship between $\ln\eta$ and $1/T$ was fitted. As shown in Figure 4, the slopes of the fitted lines are 0.27108, 0.2884, 0.46813, and 0.36374. Table 3 shows the calculated activation energy of particle movement in the modified melting-separated red mud with different CaO/Na_2O ratios in the high-temperature range. As the CaO/Na_2O increases from 2.6 to 5.0, the activation energy of particle movement in the melt shows a trend of slowly increasing–sharply increasing–decreasing, with a peak of 389.20 $kJ{\cdot}mol^{-1}$ at a CaO/Na_2O ratio of 4.0. The increase in the activation energy of particle movement in the melt is greatest when the CaO/Na_2O increases from 3.0 to 4.0, which is consistent with the variation trend of the modified melting-separated red mud samples with different CaO/Na_2O ratios; i.e., the internal determinant of melting temperature changes. The decrease in the activation energy of particle movement in the modified melting-separated red mud when the CaO/Na_2O increases from 4.0 to 5.0 is mainly due to the fact that the activation energy of particle movement is related to the degree of binding of anionic groups ($Si_xO_y^{2-}$) in the melt. The greater the degree of binding, the greater the activation energy of particle movement, and the degree of binding of anionic groups depends on the viscosity of the melt. The higher the viscosity, the greater the degree of binding of anionic groups. When the CaO/Na_2O increases to 5.0, the suitable fiber-forming temperature range for modified melting-separated red mud is 1385 to 1446 °C. Within this temperature range, the viscosity of modified melting-separated red mud with CaO/Na_2O = 5.0 is lower than that of modified melting-separated red mud CaO/Na_2O = 4.0. Therefore, the phenomenon of reduced activation energy for melt particle movement occurs when the CaO/Na_2O increases to 5.0.

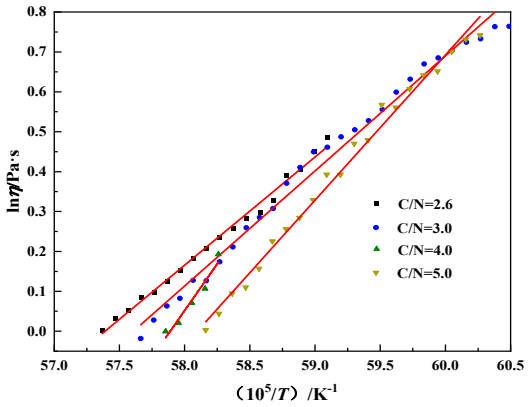

Figure 4. Fitting curves of $\ln\eta$ vs. $1/T$ for modified melting-separated red mud with different CaO/Na_2O ratios.

Table 3. Activation energy of particle movement of melting-separated red mud by different CaO/Na_2O ($kJ \cdot mol^{-1}$).

CaO/Na_2O	2.6	3.0	4.0	5.0
Activation energy of particle movement	225.38	239.78	389.20	302.4

3.2. Crystallization Performance

The formation of slag wool is a process in which modified melting-separated red mud is rapidly solidified from the long-range disordered melting state and becomes a glassy amorphous solid with long-range structural disorder; the temperature of the raw material melt during the preparation process should be above the crystallization temperature. Figure 5 shows the FactSage simulation results of the crystallization behavior of modified melting-separated red mud with different CaO/Na_2O ratios during the cooling process. Figure 5 shows that during the cooling process of modified melting-separated red mud with different CaO/Na_2O ratios, the precipitated mineral phases mainly include nepheline ($NaAlSiO_4$), anorthite ($Ca_2AlSi_2O_7$, $CaAl_2Si_2O_8$), perovskite ($CaTiO_3$), melilite ($Ca_2Al_3O_7$), and albite ($Na_2CaAl_4O_8$, $NaAlSi_3O_8$). When the CaO/Na_2O is 1.0, the dominant precipitated mineral phase of the modified melting-separated red mud during the cooling process is nepheline ($NaAlSiO_4$), followed by anorthite ($Ca_2AlSi_2O_7$), some perovskite ($CaTiO_3$), and a small amount of melilite ($Ca_2Al_3O_7$) and anorthite ($CaAl_2Si_2O_8$); when the CaO/Na_2O is 3.0, the precipitated mineral phases during the cooling of the melt are similar to those obtained with a CaO/Na_2O ratio of 1.0, but the precipitation of nepheline ($NaAlSiO_4$), anorthite ($Ca_2AlSi_2O_7$), perovskite ($CaTiO_3$), and melilite ($Ca_2Al_3O_7$) decreases, and anorthite ($CaAl_2Si_2O_8$) no longer precipitates; when the CaO/Na_2O increases to 4.0, during the cooling process, the dominant precipitated mineral phase is still nepheline ($NaAlSiO_4$), but the precipitation of nepheline ($NaAlSiO_4$), anorthite ($Ca_2AlSi_2O_7$), perovskite ($CaTiO_3$), and melilite ($Ca_2Al_3O_7$) further decreases; anorthite ($CaAl_2Si_2O_8$) no longer precipitates; and a new albite phase ($Na_2CaAl_4O_8$) precipitates and becomes the phase second in dominance only to nepheline ($NaAlSiO_4$); when the CaO/Na_2O increases to 5.0, the dominant precipitated mineral phase is albite ($Na_2CaAl_4O_8$), followed by a new albite phase ($NaAlSi_3O_8$) and a small amount of anorthite ($Ca_2AlSi_2O_7$), and nepheline ($NaAlSiO_4$) and perovskite ($CaTiO_3$) no longer precipitate. With an increase in CaO/Na_2O, the precipitation of nepheline ($NaAlSiO_4$) in which half of the Si^{4+} is replaced by Al^{3+} during the cooling process gradually decreases. When the CaO/Na_2O is above 4.0, the dominant precipitate is no longer nepheline ($NaAlSiO_4$) but albite ($Na_2CaAl_4O_8$), which means that with an increase in CaO/Na_2O, in the modified melt system, the CaO increases, the SiO_2 and Al_2O_3 decrease, and the tetrahedral network structure of [SiO_4] and [AlO_4] in the melt is broken, with a gradual transition to single short-chain Si-O and Al-O bonds filled by Na^+ and Ca^{2+} in the network voids.

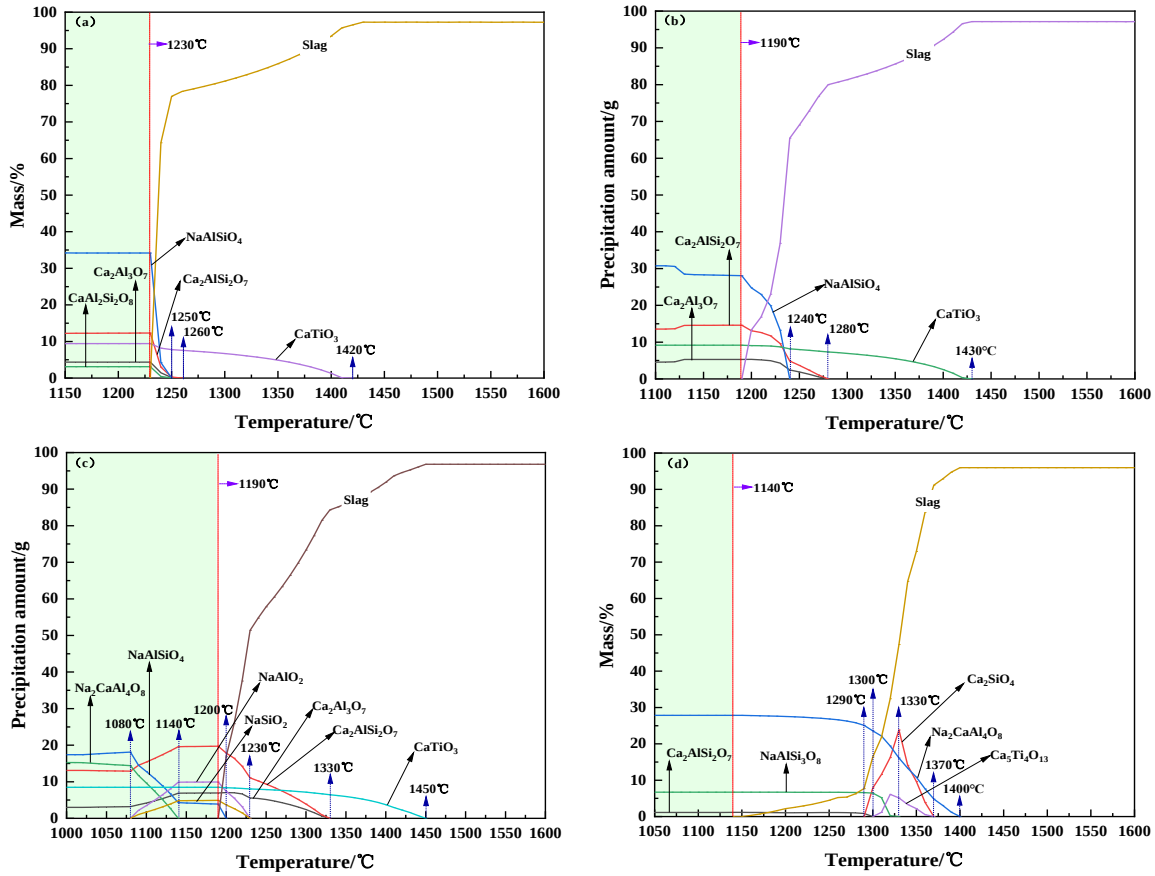

Figure 5. FactSage simulation results of precipitated mineral phases during the cooling process of modified melting-separated red mud with different CaO/Na_2O ratios. (**a**) CaO/Na_2O = 2.6, 1420 °C; (**b**) CaO/Na_2O = 3.0, 1430 °C; (**c**) CaO/Na_2O = 4.0, 1450 °C; (**d**) CaO/Na_2O = 5.0, 1400 °C.

The variation in the liquidus temperature with an increasing CaO/Na_2O ratio during the cooling process of the modified melting-separated red mud is shown in Figure 6. Figure 6 shows that with increasing CaO/Na_2O, the liquidus temperature first increases and then decreases during the cooling process, and the increase in the liquidus temperature is not significant when the CaO/Na_2O increases from 2.6 to 4.0. When CaO/Na_2O is greater than 4.0, the liquidus temperature decreases significantly. The highest liquidus temperature is reached when the CaO/Na_2O is 4.0, with a value of 1450 °C. With increasing CaO/Na_2O, the CaO content in the modified melting-separated red mud increases. CaO, as a typical non-network oxide, aggravates the melt network fracture and increases the possibility of crystallization in the melt. As a result, with increasing CaO/Na_2O, the liquidus temperature of the modified melt during the cooling process gradually increases. CaO has a significant effect on reducing the high-temperature viscosity of the melt, which improves the fluidity of the melt, causes smoother movement of the broken short-chain complexed anion groups, speeds the development of the long-range ordered structure, and makes the melt more prone to crystallization. This is also the reason that the liquidus temperature increases with increasing CaO/Na_2O during the cooling process of the modified melting-separated red mud. When CaO/Na_2O increases to 5.0, the main precipitated mineral phase during the cooling process of the modified melting-separated red mud changes from nepheline ($NaAlSiO_4$) to albite ($NaAlSiO_4$), resulting in a decrease in the energy difference between the energy of the modified melt and the main precipitated mineral phase, a weakening of the tendency to crystallize, and a decrease in the liquidus temperature [30].

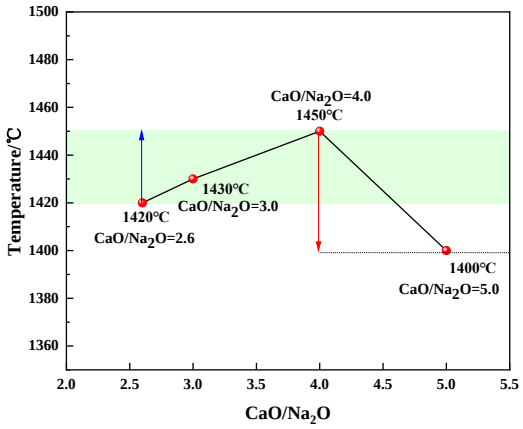

Figure 6. Distribution of the onset temperature of mineral phase precipitation in the cooling process of modified melting-separated red mud with different CaO/Na_2O ratios.

The modified melting-separated red mud samples with different CaO/Na_2O ratios were gradually heated up to 1500 °C in the tube furnace, and then the sample was kept at 1500 °C for 30 min. Then the samples were cooled in the furnace to the onset temperature of mineral phase precipitation obtained from the FactSage simulation, and the resulting melts were taken out and placed in cold water for quick cooling. The water-quenched samples were subjected to XRD analysis, and the results are shown in Figure 7. Figure 7 shows that as the CaO/Na_2O increased from 2.6 to 5.0, the temperatures of the corresponding modified melting-separated red mud samples were 1420 °C, 1430 °C, 1450 °C, and 1400 °C, respectively. The XRD patterns of the water-quenched samples show diffuse and broad peaks and no sharp diffraction peaks, and at this time, no crystals appear, which means that at CaO/Na_2O ratios of 2.6, 3.0, 4.0, and 5.0, the crystallization temperature of the modified melt was no higher than 1420 °C, 1430 °C, 1450 °C, and 1400 °C, respectively.

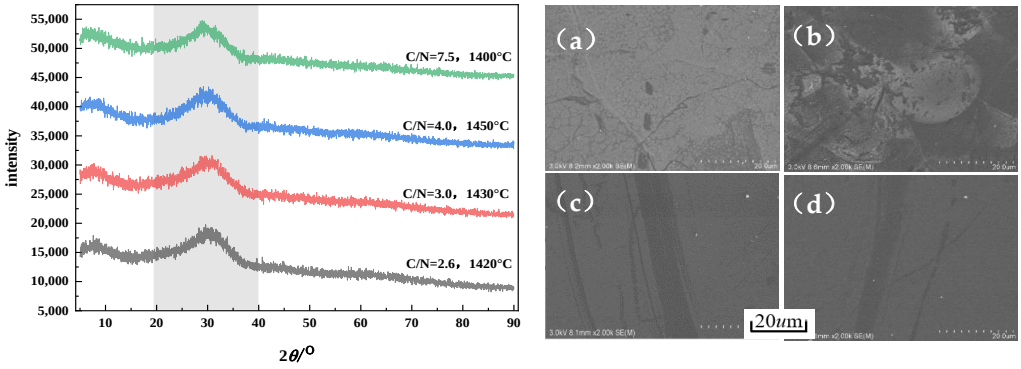

Figure 7. XRD spectra and micromorphology of water-quenched samples of modified melting-separated red mud with different CaO/Na_2O ratios. (**a**) CaO/Na_2O = 2.6, 1420 °C; (**b**) CaO/Na_2O = 3.0, 1430 °C; (**c**) CaO/Na_2O = 4.0, 1450 °C; (**d**) CaO/Na_2O = 5.0, 1400 °C.

The water quenching temperatures for the modified melting-separated red mud samples with CaO/Na_2O ratios of 2.6, 3.0, 4.0, and 5.0 were 1420 °C, 1430 °C, 1450 °C. and 1400 °C, respectively, and the samples were subjected to microscopic examination. The FESEM images show that the micromorphology of the water-quenched samples of modified melting-separated red mud with different CaO/Na_2O ratios is very smooth, and no crystals appear, which is consistent with the XRD results.

3.3. Morphology and Properties of Slag Wool

The properties of slag wool prepared by centrifugation were analyzed. Figure 8 shows the macroscopic images and micromorphology of slag wool prepared from modified melting-separated red mud with different CaO/Na_2O ratios. Figure 8 shows that the slag

wool has a smooth surface, the fibers are arranged in a crosswise fashion, the color is grayish yellow, and a small number of slag balls are inside the fibers.

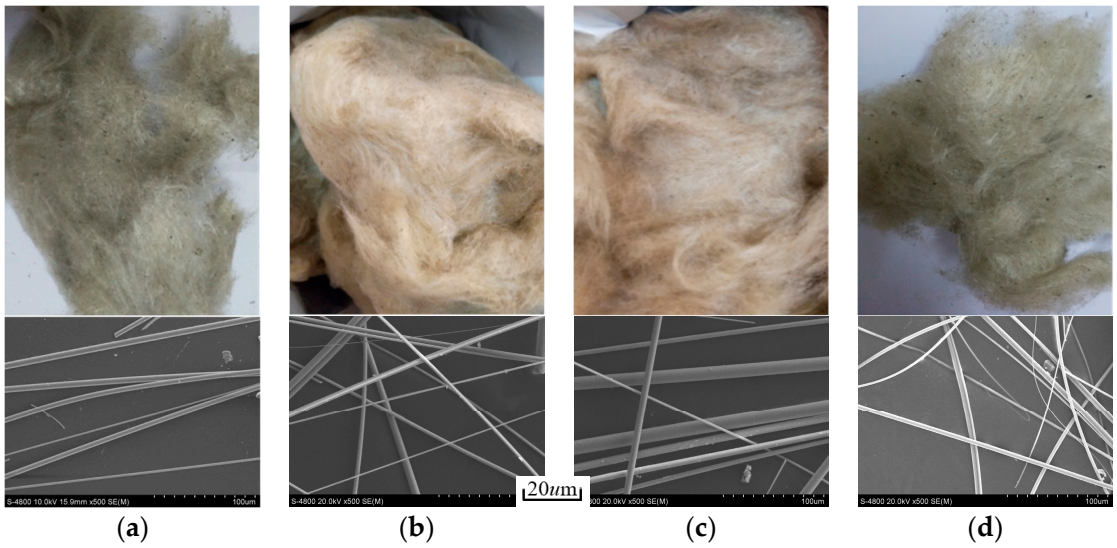

Figure 8. Macroscopic images and micromorphology of slag wool prepared from modified melting-separated red mud with different CaO/Na_2O ratios. (**a**) CaO/Na_2O = 2.6, 1420 °C; (**b**) CaO/Na_2O = 3.0, 1430 °C; (**c**) CaO/Na_2O = 4.0, 1450 °C; (**d**) CaO/Na_2O = 5.0, 1400 °C.

When slag wool is finer, the surface stress is reduced, which can reduce the possibility of fracture, and the tensile strength of the slag wool is increased. The distributions of the diameters of slag wool obtained from modified melting-separated red mud with different CaO/Na_2O ratios are shown in Figure 9a. Figure 9a shows that the diameter of the slag wool decreases with increasing CaO/Na_2O, from 6.67 μm (CaO/Na_2O = 2.6) to 5.47 μm (CaO/Na_2O = 5.0). This trend occurred because with increasing CaO/Na_2O, the CaO content in the modified melting-separated red mud system increases, which reduces the viscosity of the modified melt, making liquid filaments in the melt easy to stretch and resulting in a thinner fiber diameter [31].

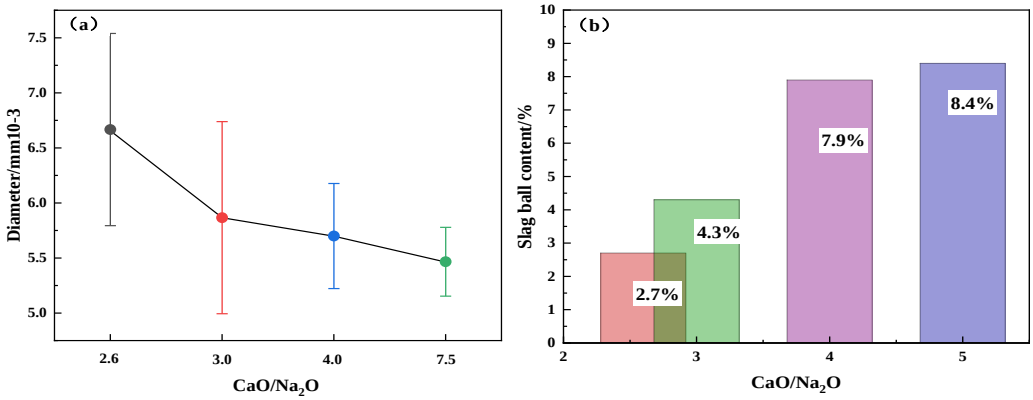

Figure 9. The diameters and slag ball content of slag wool obtained from modified melting-separated red mud with different CaO/Na_2O ratios. (**a**) The diameters; (**b**) Slag ball content.

The slag ball content refers to the ratio of the mass of slag balls with a particle diameter greater than 0.25 mm to the mass of slag wool. Slag balls are generally formed in two ways. First, during the elongation process of the filaments of the raw material melt, due to the flow of the melt from the surface of the liquid film to the heads of the liquid filaments, there is more melt at the heads of the liquid filaments; due to surface tension, the heads of the liquid filaments can shrink inward into a ball and separate from the liquid filaments, thus forming slag balls. Second, when the centrifugal force is not enough for the melt liquid filaments,

surface tension causes the liquid filaments on the surface of the liquid film to retract to form a slag ball. Except for some slag wool products that have special requirements for bulk density, the existence of slag balls can greatly reduce the quality of slag wool. The slag ball content in the slag wool obtained from modified melting-separated red mud with different CaO/Na_2O ratios is shown in Figure 9b. Figure 9b shows that the slag ball content in the slag wool shows an increasing trend as the CaO/Na_2O increases. When the CaO/Na_2O is 5.0, the slag ball content in the slag wool increases to 8.4%. With increasing CaO/Na_2O, the viscosity of the modified melting-separated red mud is effectively reduced, the time for achieving an orderly arrangement of the melt structure is shortened, the possibility of melt crystallization during the formation of the slag wool is increased, and the heads of the melt liquid filaments are increased, which increases the sites for slag ball formation; therefore, the slag ball content in the slag wool increases with increasing CaO/Na_2O.

4. Conclusions

(1) For CaO/Na_2O ratios from 2.6 to 5.0, the viscosity of the modified melting-separated red mud decreases with increasing temperature; the activation energy of the particle movement of the modified melting-separated red mud shows a trend of slowly increasing–sharply increasing–decreasing with increasing CaO/Na_2O, which is consistent with the trend of the melting temperature of modified melting-separated red mud.

(2) The suitable fiber-forming temperature interval of modified melting-separated red mud shows a trend of increasing–decreasing–increasing with increasing CaO/Na_2O. Considering the feasibility of preparing slag wool from modified melting-separated red mud, the CaO/Na_2O ratio in the modified raw material system should not be higher than 3.0.

(3) For CaO/Na_2O ratios from 2.6 to 5.0, the precipitated mineral phases of modified melting-separated red mud during the cooling process mainly include nepheline ($NaAlSiO_4$), anorthite ($Ca_2AlSi_2O_7$, $CaAl_2Si_2O_8$), perovskite ($CaTiO_3$), melilite ($Ca_2Al_3O_7$), and albite ($Na_2CaAl_4O_8$, $NaAlSi_3O_8$), and the crystallization temperature first increases and then decreases. When the CaO/Na_2O is 4.0, the maximum crystallization temperature of the modified melting-separated red mud during the cooling process is 1450 °C, and the increase in the crystallization temperature of the melt is not significant when the CaO/Na_2O increases from 2.6 to 4.0. When the CaO/Na_2O is greater than 4.0, the onset crystallization temperature of the melt decreases significantly.

(4) The slag wool prepared from modified melting-separated red mud with different CaO/Na_2O ratios has a smooth surface and a grayish yellow color, and the fibers are arranged crosswise and contain a small amount of slag balls. The diameters of the slag balls are all less than 7 μm, with an average diameter of 5.93 μm, and the slag ball content is 5.83%. With increasing CaO/Na_2O, the diameter of the slag wool gradually decreases, but the variation is insignificant, and the slag ball content gradually increases, with a significant increase when the CaO/Na_2O is greater than 3.0.

Author Contributions: Conceptualization, P.D. and Y.Z.; methodology, P.D.; software, L.X.; validation, Y.L.; writing—review and editing, P.D. All authors have read and agreed to the published version of the manuscript.

Funding: This study was funded by National Natural Science Foundation of China (U20A20271).

Data Availability Statement: Data are contained within the article.

Conflicts of Interest: The authors declare no conflict of interest.

References

1. Wang, S.; Jin, H.; Deng, Y.; Xiao, Y. Comprehensive utilization status of red mud in China: A critical review. *J. Clean. Prod.* **2021**, *289*, 125136. [CrossRef]
2. Lu, G.Z.; Zhang, T.A.; Ma, L.N.; Wang, Y.X.; Zhang, W.G.; Zhang, Z.M.; Wang, L. Utilization of Baver red mud by a calcification-carbonation method using calcium aluminate hydrate as a calcium source. *Hydrometallurgy* **2019**, *188*, 248–255. [CrossRef]
3. Wang, Q.Q.; Chen, Z.T.; Li, J.Q.; Zheng, H.N.; Wang, T.H. Recovery of aluminum and iron from red mud by low temperature roasting with sodium pyrosulfate. *Chin. J. Nonferrous Met.* **2023**, *23*, 1–16.
4. Li, Y.; Ou, D.Y. Research on development countermeasures of bulk solid waste resource utilization under the background of low-carbon. *Jiangxi Build. Mater.* **2022**, *28*, 5–8+12.
5. Li, S.; Zhou, B.; Liu, W.C.; Zhou, X.F.; Wang, S. Status-quo, problems and solutions of red mud comprehensive utilization. *China Nonferrous Metall.* **2022**, *51*, 32–36. [CrossRef]
6. Xie, L.; Zhang, T.; Lv, G.; Yang, J.; Wang, Y. The effect of NaOH on the direct calcification-carbonation method for processing of bayer process red mud. *Green Process. Synth.* **2017**, *70*, 546–551. [CrossRef]
7. Andras, G.; Nora, K.; Beatrix, T. The red mud accident in ajka (hungary): Characterization and potential health effects of fugitive dust. *Environ. Sci. Technol. EST* **2011**, *45*, 1608–1615.
8. Pan, X.; Wu, H.; Lv, Z.; Yu, H.; Tu, G. Research status and prospect of iron and aluminum recovery technology from red mud. *Chin. J. Nonferrous Met.* **2023**, *23*, 1–32.
9. Liu, C.; Ma, S.; Zheng, S.; Luo, Y.; Ding, J.; Wang, X.; Zhang, Y. Combined treatment of red mud and coal fly ash by a hydro-chemical process. *Hydrometallurgy* **2018**, *175*, 224–231. [CrossRef]
10. Zhang, J.; Liu, S.; Yao, Z.; Wu, S.; Jiang, H.; Liang, M.; Qiao, Y. Environmental aspects and pavement properties of red mud waste as the replacement of mineral filler in asphalt mixture. *Constr. Build. Mater.* **2018**, *180*, 605–613. [CrossRef]
11. Chen, Z.; Wang, M.; Wang, H.; Liu, L.; Wang, X. ANN-based structure-viscosity relationship model of multicomponent slags for production design in mineral wool. *Constr. Build. Mater.* **2022**, *319*, 126010. [CrossRef]
12. Li, Z.H. Fibering Mechanism of Modified Molten Blast Furnace Slag and Experimental Research. Ph.D. Thesis, Northeastern University, Shenyang, China, 2018.
13. Koroli, M.A.; Ivanisova, A.R. Thermal insulation of engineering structures with mineral wool based on basalt fiber. In Proceedings of the 7th International Seminar on Advances in Materials Science and Engineering, Changsha, China, 21–23 May 2021.
14. Pavlin, M.; König, K.; König, J.; Javornik, U.; Ducman, V. Sustainable alkali-activated slag binders based on alternative activators sourced from mineral wool and glass waste. *Front. Mater.* **2022**, *9*, 902139. [CrossRef]
15. Kostadinović, D.; Jovanović, M.; Bakić, V.; Stepanić, N.; Todorović, M. Experimental investigation of summer thermal performance of the green roof system with mineral wool substrate. *Build. Environ.* **2022**, *217*, 109061. [CrossRef]
16. Pavlin, M.; Horvat, B.; Ducman, V. Preparation of façade panels based on alkali-activated waste mineral wool, their characterization, and durability aspects. *Int. J. Appl. Ceram. Technol.* **2022**, *19*, 1227–1234. [CrossRef]
17. Li, Z.J. Blast Furnace Slag Wool Used as Soilless Culture Substrates on Flowers. Ph.D. Thesis, North China University of Science and Technology, Tangshan, China, 2019.
18. Balomenos, E.; Giannopoulou, I.; Gerogiorgis, D.; Panias, D.; Paspaliaris, I. Resource-efficient and economically viable pyrometallurgical processing of industrial ferrous by-products. *Waste Biomass Valorization* **2013**, *5*, 333–342. [CrossRef]
19. Balomenos, E.; Panias, D. Iron recovery and production of high added value products from the metallurgical by-products of primary aluminium and ferro-nickel industries. In Proceedings of the 3rd International Slag Valorisation Symposium, Leuven, Belgium, 19–20 March 2013.
20. Kim, Y.; Kim, M.; Sohn, J.; Park, H. Applicability of gold tailings, waste limestone, red mud, and ferronickel slag for producing glass fibers. *J. Clean. Prod.* **2018**, *203*, 957–965. [CrossRef]
21. Chen, Z.; Wang, H.; Wang, M.; Wu, W.; Liu, L.; Wang, X. Simulation and experimental investigation on one-step process for recovery of valuable metals and preparation of clean mineral wool from red mud. *J. Clean. Prod.* **2018**, *380*, 134982. [CrossRef]
22. Bernd, F.; Frank, K.; Efthymios, B.; Dimitrios, P. *Slag Design for Glass Fiber Production from Red Mud after Iron Removal*; RWTH Aachen University: Berlin, Germany, 2016.
23. Du, P.; Zhang, Y.; Long, Y.; Xing, L. Preparation of CaO-SiO_2-Al_2O_3 inorganic fibers from melting-separated red mud. *High Temp. Mater. Process.* **2023**, *42*, 20220272. [CrossRef]
24. Zhao, C.G. Fluidity and Structure of CaO-SiO-MgO-Al_2O_3-FeO Bosh Slag in Blast Furnace. Master's Thesis, University of Science and Technology Liaoning, Anshan, China, 2016.
25. Turkdogen, E.T. *Physicochemical Properties of Molten Slags and Glasses*, 1st ed.; The Metals Society: London, UK, 1983; pp. 81–85.
26. He, K.Y. *Physical Chemistry of Silicate*, 1st ed.; Wuhan University of Technology Press: Wuhan, China, 2010; pp. 227–228.
27. Liang, Z.Y.; Ning, X.J. Analysis of viscosity and thermodynamic properties of high alumina slag. *Met. World* **2019**, *26*, 16–19+35.
28. Du, P.P. Mechanism and Experiment Research of Centrifugal Spinning Method of Blast Slag. Master's Thesis, North China University of Science and Technology, Tangshan, China, 2016.
29. Fan, X.Y.; Zhang, J.L.; Xu, R.Z.; Jiao, K.; Wang, K. Effect of B_2O_3 on fluidity of low MgO slag containing titanium. *J. Cent. South Univ. (Sci. Technol.)* **2018**, *49*, 1863–1868.

30. Lu, P.W. *Fundamentals of Inorganic Materials Science*, 1st ed.; Wuhan University of Technology Press: Wuhan, China, 2010; pp. 264–271.
31. Zhang, Z.Q. Study on Technology of Fiber Formation of Molten Blast Furnace Slag and Fiber Products. Ph.D. Thesis, Yanshan University, Qinhuangdao, China, 2015.

Disclaimer/Publisher's Note: The statements, opinions and data contained in all publications are solely those of the individual author(s) and contributor(s) and not of MDPI and/or the editor(s). MDPI and/or the editor(s) disclaim responsibility for any injury to people or property resulting from any ideas, methods, instructions or products referred to in the content.